Comparison Between 2D and 3D Modelling of Induction Machine Using Finite Element Method

Zelmira FERKOVA

Department of Electrical Engineering and Mechatronics, Faculty of Electrical Engineering and Informatics, Technical University of Kosice, Letna 9, 042 00 Kosice, Slovak Republic

zelmira.ferkova@tuke.sk

DOI: 10.15598/aeee.v13i2.1346

Abstract. *The paper compares two different ways (2D and 3D) of modelling of two-phase squirrel-cage induction machine using the finite element method (FEM). It focuses mainly on differences between starting characteristics given from both types of the model. It also discusses influence of skew rotor slots on harmonic content in air gap flux density and summarizes some issues of both approaches.*

Keywords

Density, finite element method, flux, harmonics, torque, two-phase induction motor.

1. Introduction

Three-phase induction machines are supplied by three-phase symmetrical voltage. Windings of the motors are arranged within the stator and mutually shifted by 120 electrical degrees. The machines operate with circular magnetic fields. Single-phase motors have two windings (phases) inside their stators mutually shifted by 90 electrical degrees and have usually aluminum squirrel-cage. One of the stator winding works as main phase and the second one is used as auxiliary phase. Both phases are supplied from a single-phase power source. Time shift of the current flowing through the auxiliary winding is usually achieved by in series connected capacitor. This construction generates an elliptic magnetic field producing torque including forward and backward components [1], [2], [3].

If both main and auxiliary windings are identical and supplied by symmetrical two-phase voltage, produced is circular magnetic field with balanced torque (as given by three-phase induction machine)[4], [5], [6], [7], [8]. This type of machine is used for analysis (comparison) because it has longer end-windings as compared with three-phase induction machine.

The main issues of 2D and 3D modelling of induction machine have been already discussed at global scale in common literature but comparison between specific results from those models is still lacking [9], [10] [11], [12]. The usual problem is to estimate the influence of overhang part of the winding or edge effect on the resulting magnetic field. In this article a small (and "short") motor is discussed. In literature only motors of higher power are analysed and discussed.

The main issue of this paper is to investigate the influence of skewed rotor slots and ends of windings on results and validate the 2D model of this type of induction machine even in case of non-axial symmetric rotor. Full-scale FE models (2D/3D) used for this purpose take into consideration all necessary features: the geometry, non-linearity of magnetic material and transient supply with moving rotor. The studied machine is an ordinary industrial single-phase induction machine redesigned for two-phase supply with $Q_1 = 24$ slots on the stator. It has aluminum squirrel cage with $Q_2 = 30$ round trapezoidal rotor bars. The machine may be classified as "short" with relatively high ratio between rotor diameter D_r and the machine's length l_{FE}. Nominal parameters and main geometrical dimensions are shown in Tab. 1.

Tab. 1: Main parameters of analyzed two-phase induction machine.

Parameter		Value	Unit
Rated power	P_r	50	W
Rated voltage (two-phase)	U_r	115	V
Rated speed	n_r	2400	r/min
Number of slots	Q_1/Q_2	24/30	-
Rotor diameter	D_r	$55.4 \cdot 10^{-3}$	m
Rotor length	l_{FE}	$22.3 \cdot 10^{-3}$	m

2. FE Model of Studied Motor

Both 2D and 3D models (Fig. 2 and Fig. 3) calculate the start-up characteristic with no external load set on the shaft. The load strongly alters the back magneto-motive force (mmf) of the rotor and consequently the air gap magnetic field. Its harmonic content may be used as a measure of influence of skewed rotor bars. The power supply is considered as two-phase symmetrical voltage including no time harmonics.

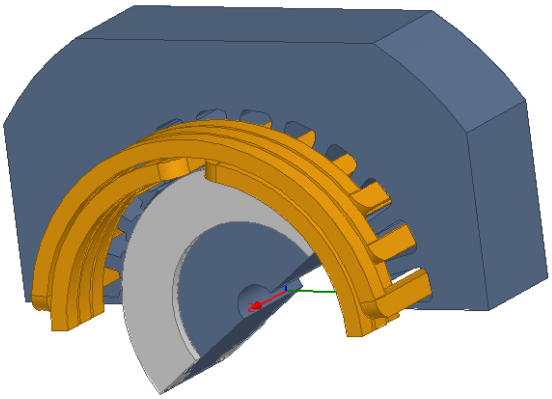

Fig. 1: 3D model of studied machine.

As seen, the advantage of half-symmetry is used to make the computation time as short as possible. The stator coils are simplified to one single piece of copper wire with hypothetical number of turns. It brings significant reduction of the model (density of computation mesh). While the 3D solution works with 119724 mesh elements the 2D model is meshed only with 7912 elements (provides practically the same results as given from the same model with 90000 elements). Unlike the 2D model, the 3D model considers real overhang part of windings together with real skewed rotor bars in calculation. In 2D model the ends of winding and skewed slots were considered as added leakage inductances computed in RMxprt. RMxprt (Rotational Machine Expert) works with an analytical method of designing electric machines.

According to the electrical motor design tradition [14], leakage inductance can by divided into following leakage inductances:

$$L_\sigma = L_\delta + L_u + L_d + L_w + L_{sq}, \tag{1}$$

where L_σ - air gap leakage inductance, L_u - slot leakage inductance, L_d - tooth tip leakage inductance, L_w - end winding inductance, L_{sq} - skew leakage inductance.

The investigated flux density in time $t = 0.03$ s is shown in Fig. 2 and Fig. 3.

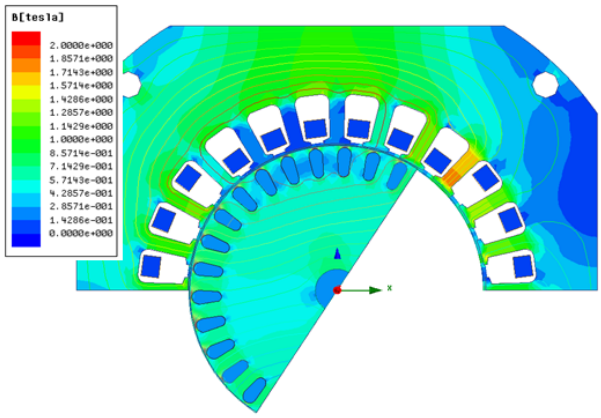

Fig. 2: 2D model of studied machine – flux density distribution.

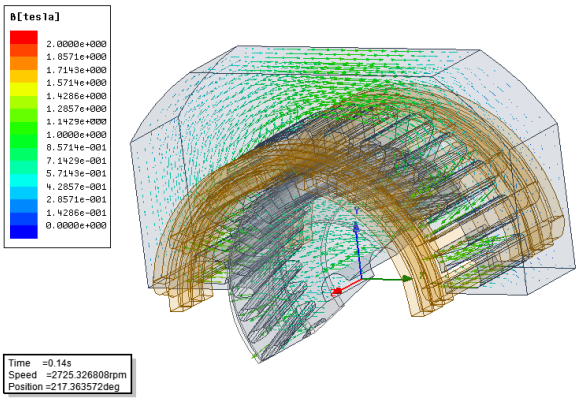

(a)

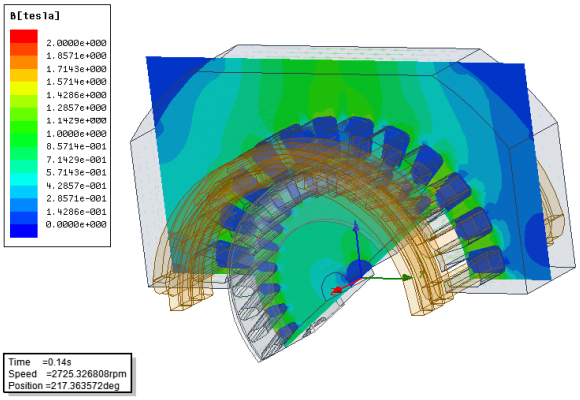

(b)

Fig. 3: (a) B-vectors and (b) nodal form of magnetic field.

As obvious from Fig. 2 and Fig. 3 both models give relatively same results (from saturation point of view), but the most significant difference lies in the possibility to consider the overhang part of winding and skew rotor slots affecting torque ripple and input current. Calculated current characteristics for individual phases together with torque and speed characteristics are illustrated in Fig. 4, Fig. 5 and Fig. 6.

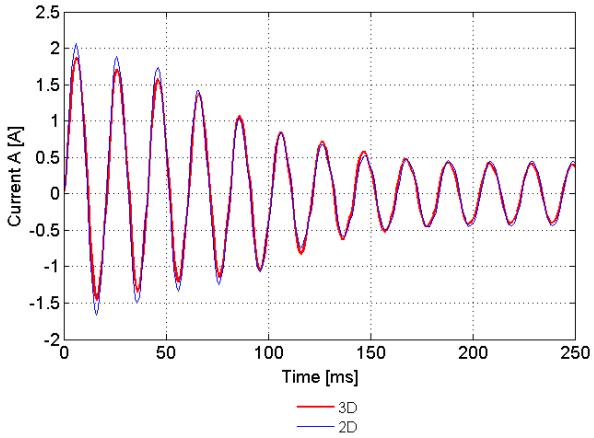

(a)

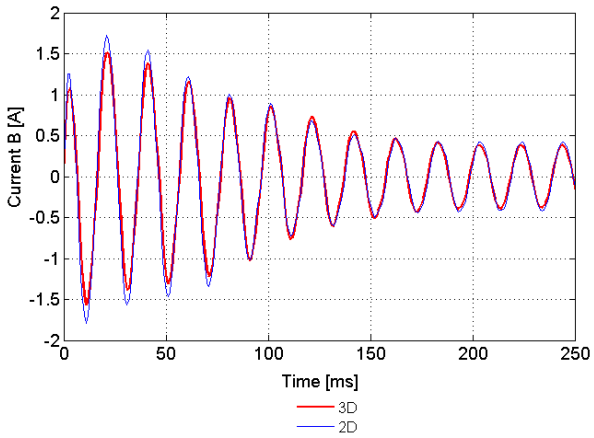

(b)

Fig. 4: Comparison of starting current characteristics.

The current given from 3D model is compared with 2D (Fig. 4) model slightly reduced by skewed (1.5 of slot pitch) rotor slots and partial inaccuracy of set leakage winding parameters.

The influence of this feature can be also seen in Fig. 5 comparing starting no-load torque characteristic for 3D, 2D and 2D model without added leakage inductance. The common way of 2D simulation does not take into consideration the stator end-windings.

The start-up procedure was simulated as a direct connection to the power grid. Oscillations in the resulting torque waveforms are caused by slots' openings, partial winding unbalance of placing and some numerical matters.

Differences between the 2D and 3D models are clearly seen in the torque-slip characteristics (see Fig. 6). The red curve (3D) obviously lies much closer to the measurement. It is because the machine is relatively "short" and the edge effects are (not considered in 2D) not negligible.

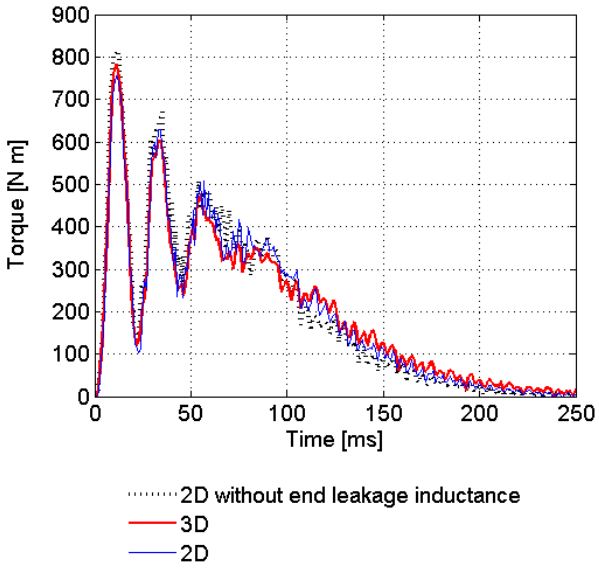

Fig. 5: Comparison of transient torque characteristics.

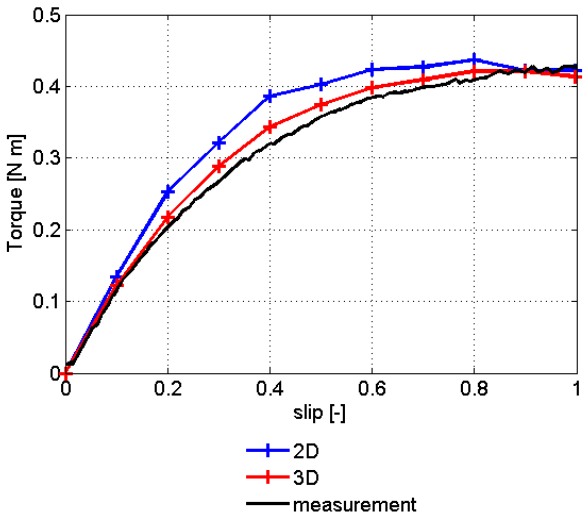

Fig. 6: Steady-state (torque-slip) torque characteristics.

3. Air Gap Flux Density

The sleek start of an induction machine is considerably affected by an air gap magnetic field containing space harmonics. These are caused by slot leakage saturation, together with slot openings and winding construction, and produce parasitic components in steady state torque characteristic [13], [15], [16], [17].

Using 2D and 3D finite element analysis (FEA), the air gap field distribution may be easily calculated and properly compared to evaluate the influence of skewed rotor bars.

The air gap magnetic field calculated for two different loaded states are shown in Fig. 7 and Fig. 8. While the first speed of 2700 r/min relates to slip 0.1 and av-

erage torque $T = 0.13$ N·m, the second one, 1500 r/min refers to slip 0.5 of average torque $T = 0.4$ N·m. The comparison between them is seen in Fig. 9 and Fig. 10. In 3D analysis the air gap flux density is calculated on circle path in the middle of the motor's length. As seen in Fig. 7 and Fig. 8 the skew slots slightly lower distortion of the fundamental wave by space harmonic components.

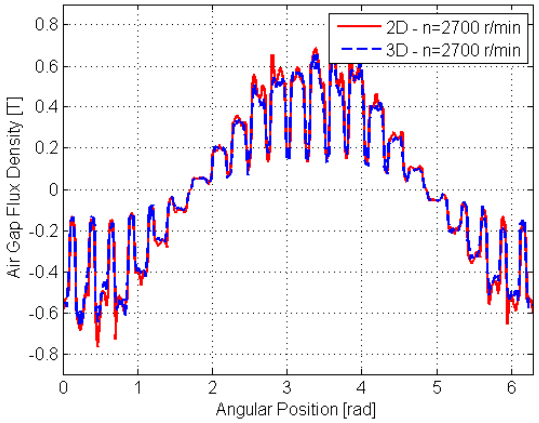

Fig. 7: The air gap flux density $n = 2700$ r/min.

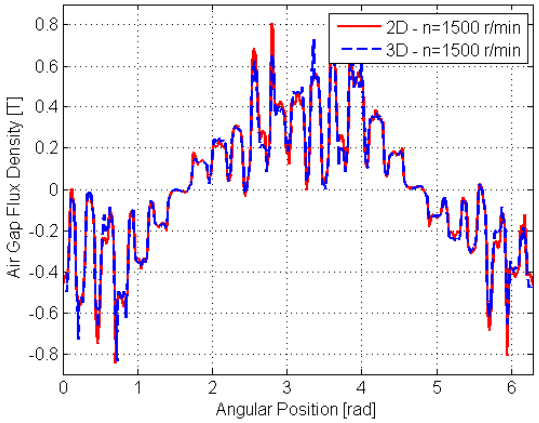

Fig. 8: Air gap flux density $n = 1500$ r/min.

The resulting amplitude spectrums from Fig. 9 and Fig. 10 (given from 3D and 2D model) are shown in Fig. 11, Fig. 12, Fig. 13 and Fig. 14. Amplitudes of harmonic components of all presented spectrums are referred to the amplitude of its fundamental wave.

The most significant 23^{th} and 25^{th} components (Fig. 11 and Fig. 12) and their linear multiples ν_1 are caused by stator slots according to Eq. (2).

$$\nu_1 = c\frac{Q_1}{p} \pm 1 = c\frac{24}{1} \pm 1 \quad \text{for} \quad c = 1, 2, 3, \ldots . \tag{2}$$

The rising machine's load (higher slip) generates stronger back mmf of the rotor, increasing values of

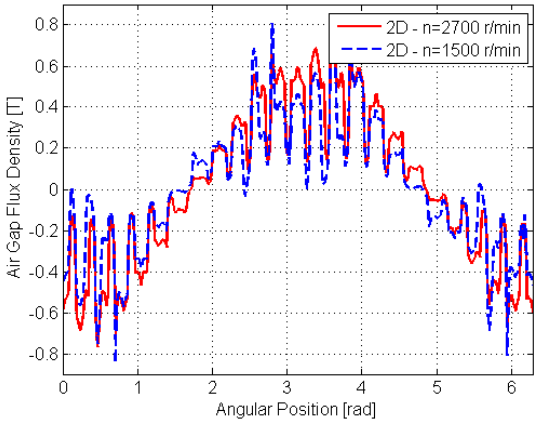

Fig. 9: The air gap flux density 2D calculation (comparison).

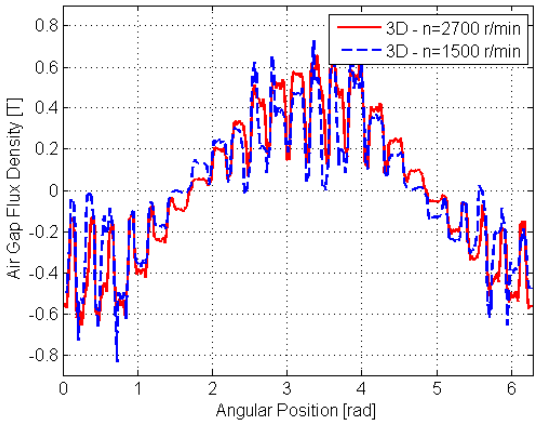

Fig. 10: The air gap flux density 3D (comparison).

the 29^{th} and 31^{st} harmonic components (Fig. 13 and Fig. 14) and their linear multiples ν_2. Those are generally caused by rotor slots according to Eq. (3).

$$\nu_2 = c\frac{Q_2}{p} \pm 1 = c\frac{30}{1} \pm 1. \tag{3}$$

While the stator winding is placed in only one layer, no chording is possible. This makes the winding worse distributed, and produces amounts of unsuppressed harmonic component of orders ν_s Eq. (4).

$$\nu_s = 2mc \pm 1. \tag{4}$$

The 3^{rd}, 5^{th}, 7^{th} and 9^{th} orders from Eq. (4) in Fig. 13 and Fig. 14 therefore take place mainly in case of higher machine's load producing stronger stator mmf.

According to Fig. 10 and Fig. 11 there is almost no difference in low torque air gap flux density resulting from 2D/3D models. More significant differences may be found only in widely loaded operating states, where the higher stator current act more distinctly.

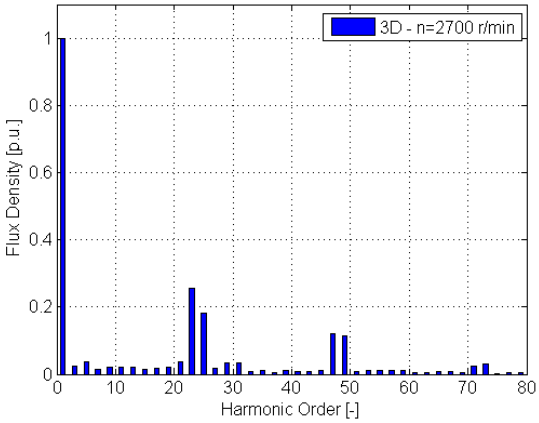

Fig. 11: The amplitude frequency spectrum of the blue curve (3D $n = 2700$ r/min) depicted in Fig. 7.

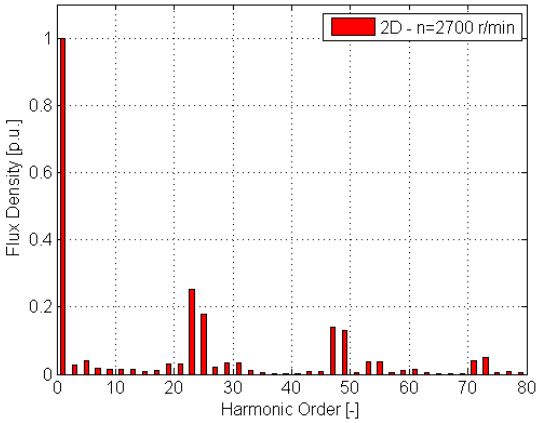

Fig. 12: The amplitude frequency spectrum of the red curve (2D $n = 2700$ r/min) depicted in Fig. 7.

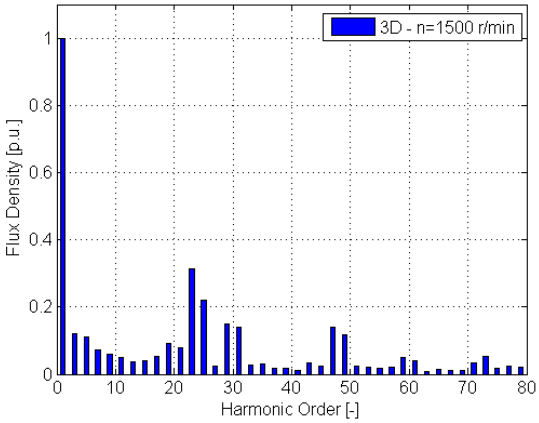

Fig. 13: The amplitude frequency spectrum of the blue curve (3D $n = 1500$ rpm) depicted in Fig. 8.

The comparison between the most significant harmonic components is listed in Tab. 2.

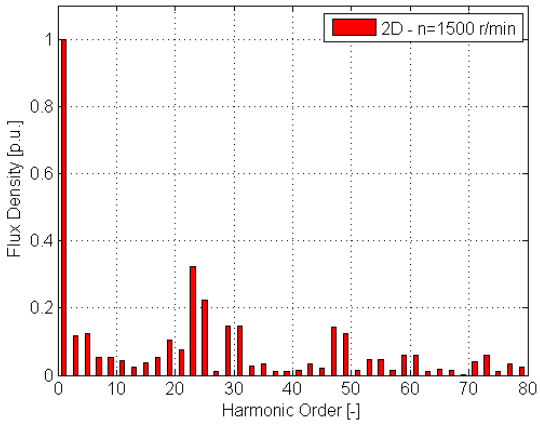

Fig. 14: The amplitude frequency spectrum of the red curve (2D $n = 1500$ rpm) depicted in Fig. 8.

Tab. 2: Amplitudes of most significant harmonics.

Harmonic Order	n=2700 [r/min]		n=1500 [r/min]	
	B [p.u.]		B [p.u.]	
	2D	3D	2D	3D
3rd	0.027	0.026	0.116	0.122
5th	0.041	0.037	0.123	0.111
7th	0.018	0.013	0.052	0.071
9th	0.014	0.022	0.052	0.063
11th	0.015	0.021	0.045	0.052
23rd	0.252	0.255	0.335	0.313
25th	0.181	0.182	0.226	0.224
29th	0.035	0.033	0.147	0.151
31st	0.034	0.033	0.148	0.143

The results indicate relatively good agreement between the two models. The only considerable difference can be seen at higher load in stator slots harmonic components which are lower due to skewed rotor bars.

4. Experimental Measurement

All theoretical statements are supported by laboratory measurement of the discussed two-phase squirrel-cage induction machine. The testing laboratory stand scheme can be seen in Fig. 15.

The machine is supplied from a symmetrical two-phase power source. Currents (Fig. 16) and voltages are measured with current probes. The torque developed during the test is measured with torsional torque sensor (Staiger Mohilo typ: IT10/1Nm).

Measured current waveforms are shown in Fig. 16 and the corresponding calculated current waveforms are illustrated in Fig. 17. The supply source used in the experiment was relatively soft and this is the reason why the amplitude of the measured and calculated currents during start-up is slightly lower than the simulated waveforms (Fig. 4).

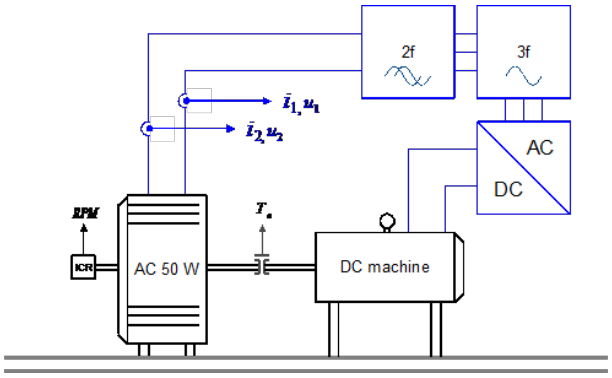

Fig. 15: The assessment of testing stand.

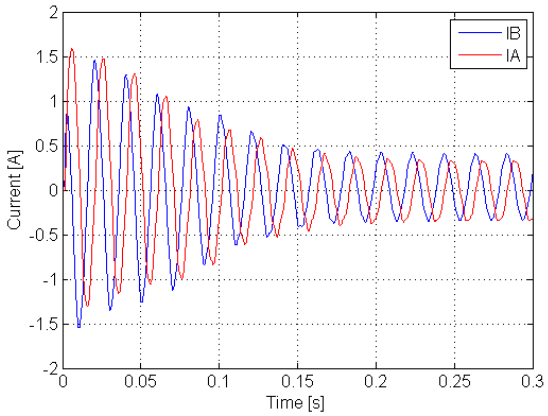

Fig. 16: The measured current.

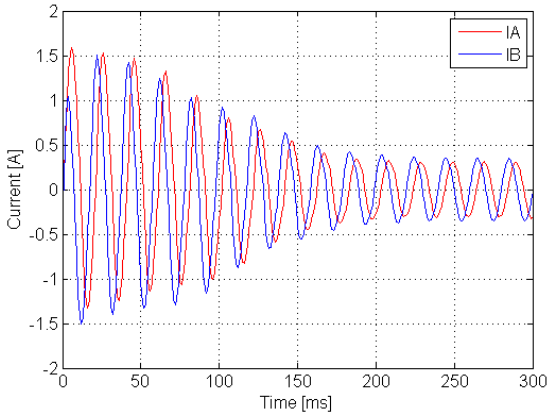

Fig. 17: The simulated current.

5. Conclusion

From the comparison of currents, torques and air gap flux density distribution it is clear that the differences between results of 2D and 3D models are relatively small but must be considered. In case of preliminary and glance calculation the 2D model gives satisfying results. It is therefore acceptable to simulate the low power induction machines with non-axial symmetric and relatively short rotor only by using 2D FEM models.

Since, the 3D version of the model is more suitable for the calculation it does not increase the result's accuracy in the same range as it extends the computation time.

Acknowledgment

This work were supported by research project No. SK-CZ-2013-0065: Multivariable Physical Calculation Applicable to Electric Drives and research project No: VEGA 1/0121/15 " Electric Drive with High Frequency Two-Phase Asynchronous Motor".

References

[1] ALSHAMASIN, M. Towards Economic Single-Phase Motor. *Energy and Power Engineering*. 2013, vol. 5, iss. 9, pp. 528–536. ISSN 1947-3818. DOI: 10.4236/epe.2013.59058.

[2] HRABOVCOVA, V. and P. RAFAJDUS. Radial magnetic forces of single-phase permanent split-capacitor motor. *Journal of Electrical Engineering*. 2006, vol. 57, no. 4, pp. 185–192. ISSN 1335-3632.

[3] DOBRUCKY, B., M. FRIVALDSKY, M. PRAZENICA, P. SPANIK, V. HRABOVCOVA, P. SEKERAK, L. KALAMEN and P. RAFAJDUS. Two-phase power electronic drive with split — Single-phase induction motor. In: *IECON 2010 - 36th Annual Conference on IEEE Industrial Electronics Society*. Glendale: IEEE, 2010, pp. 1683–1688. ISBN 978-1-4244-5225-5. DOI: 10.1109/IECON.2010.5675430.

[4] POPESCU, M., E. DEMETER, D. MICU, V. NAVRAPESCU and T. JOKINEN. Analysis of a voltage regulator for a two-phase induction motor drive. In: *IEEE International Electric Machines and Drives Conference. IEMDC'99*. Seattle: IEEE, 1999, pp. 658–660. ISBN 0-7803-5293-9. DOI: 10.1109/IEMDC.1999.769205.

[5] KUMSUWAN, Y., W. SRIRATTANAWICHAIKUL and S. PREMRUDEEPREECHACHARN. Analysis of two-phase induction motor using dynamic model based on MATLAB/Simulink. *Asian Journal on Energy and Environment*. 2010, vol. 11, iss. 1, pp. 48–59. ISSN 1513-4121.

[6] CRACIUNAS, G. *Field oriented control of a two phase induction motor* [online]. 2003. Available

at: http://ace.ucv.ro/sintes11/Volume1/1AUTOMATION/A07_Craciunas_Gabriela_2.pdf.

[7] ABDEL-RAHIM, N. M. B. and A. SHALTOUT. An Unsymmetrical Two-Phase Induction Motor Drive With Slip-Frequency Control. *IEEE Transactions on Energy Conversion*. 2009, vol. 24, iss. 3, pp. 608–616. ISSN 0885-8969. DOI: 10.1109/TEC.2009.2026599.

[8] SEKERAK, P., V. HRABOVCOVA, P. RAFAJDUS, L. KALAMEN and M. PRAZENICA. Behaviour of Two-Phase Machine under Non-Harmonic Supply. In: *XII International Ph.D. workshop, OWD 2010*. Wisla: Organizing Committee of the Symposium PPEE, 2010, pp. 181–185. ISBN 83-922242-7-2.

[9] THOMAS, P., J.-P. DUCREUX, F. PIRIOU, B. BOUALEM and P. DZIWNIEL. Comparison between two approaches to model induction machines with skewed slots. *IEEE Transactions on Magnetics*. 2000, vol. 36, iss. 4, pp. 1453–1457. ISSN 0018-9464. DOI: 10.1109/20.877712.

[10] WENDLING, P., A. PERREGAUX, A. AKABAR, Y. LEFLOCH, P. LOMBARD and L. SADI-HADDAD. Two techniques for modeling an induction motor with skewed slots with a time-stepping 2D-3D finite element method. In: *IEEE Electric Ship Technologies Symposium, 2005*. Philadelphia: IEEE, 2005, pp. 463–467. ISBN 0-7803-9259-0. DOI: 10.1109/ESTS.2005.1524716.

[11] LAI, H. C. Comparison of 2D and 3D finite element modelling results of a skewed induction machine. In: *International Conference on Power Electronics Machines and Drives*. London: IEEE, 2002, pp. 365–368. ISBN 0-85296-747-0. DOI: 10.1049/cp:20020144.

[12] HENZL, C., P. KACOR and J. PALECEK. Investigation of Magnetic Field in the Subway Station. *Advances in Electrical and Electronic Engineering*. 2006, vol. 5, no. 1–2, pp. 254–257. ISSN 1336-1376.

[13] DARDA, R. and K. HRUSKA. Electromagnetic and constructional design of welded induction machine. In: *13th International Symposium, MECHATRONIKA 2010*. Trencianske Teplice: IEEE, 2010, pp. 59–61. ISBN 978-1-4244-7962-7.

[14] PYRHONEN, J., T. JOKINEN and V. HRABOVCOVA. *Design of Rotating Electrical Machines*. Chichester: John Wiley, 2009. ISBN 978-047-0740-088.

[15] SOBRA, J., V. KINDL and B. SKALA. Determination of the force caused by broken rotor bar and static eccentricity in an induction machine. In: *ELEKTRO 2014*. Rajecke Teplice: IEEE, 2014, pp. 375–378. ISBN 978-1-4799-3720-2. DOI: 10.1109/ELEKTRO.2014.6848921.

[16] HRUSKA, K. and V. KINDL. A comprehensive approach to calculation of the air gap magnetic flux density in induction machines with eccentrically placed rotor. In: *16th International Conference on Mechatronics - MECHATRONIKA 2014*. Brno: IEEE, 2014, pp. 52–59. ISBN 978-80-214-4817-9. DOI: 10.1109/MECHATRONIKA.2014.7018235.

[17] DAUT, I., K. ANAYET and S. TIRAPATHY. Design and modeling of induction motor using opera 2D based on aluminum material. In: *3rd International Conference on Energy and Environment (ICEE)*. Malacca: IEEE, 2009, pp. 94–97. ISBN 978-1-4244-5144-9. DOI: 10.1109/ICEENVIRON.2009.5398664.

About Authors

Zelmira FERKOVA graduated in electrical engineering from the Technical University of Kosice in 1982 and received her Ph.D. degree in 1994. At present she is active as associate professor at the Department of Electrical Engineering and Mechatronics, Faculty of Electrical Engineering and Informatics, Technical University of Kosice. Her professional area covers design of electrical machines and their performance.